Journal of Zhejiang University-SCIENCE B (Biomedicine & Biotechnology) 2025 26(3):286-301
www.jzus.zju.edu.cn; www.springer.com/journal/11585
E-mail: jzus_b@zju.edu.cn

Research Article

https://doi.org/10.1631/jzus.B2300777

Check for updates

Promising protective treatment potential of endophytic bacterium *Rhizobium aegyptiacum* for ulcerative colitis in rats

Engy ELEKHNAWY[1*✉], Duaa ELIWA[2*], Sebaey MAHGOUB[3], Sameh MAGDELDIN[3,4], Ehssan MOGLAD[5], Sarah IBRAHIM[6], Asmaa Ramadan AZZAM[6], Rehab AHMED[7], Walaa A. NEGM[2✉]

[1]*Pharmaceutical Microbiology Department, Faculty of Pharmacy, Tanta University, Tanta 31527, Egypt*
[2]*Department of Pharmacognosy, Faculty of Pharmacy, Tanta University, Tanta 31527, Egypt*
[3]*Proteomics and Metabolomics Research Program, Department of Basic Research, Children's Cancer Hospital 57357, Cairo 11441, Egypt*
[4]*Department of Physiology, Faculty of Veterinary Medicine, Suez Canal University, Ismailia 41522, Egypt*
[5]*Department of Pharmaceutics, College of Pharmacy, Prince Sattam bin Abdulaziz University, P.O. Box 173, Alkharj 11942, Saudi Arabia*
[6]*Human Anatomy and Embryology Department, Faculty of Medicine, Tanta University, Tanta 31527, Egypt*
[7]*Division of Microbiology, Immunology and Biotechnology, Department of Natural Products and Alternative Medicine, Faculty of Pharmacy, University of Tabuk, Tabuk 47713, Saudi Arabia*

Abstract: Ulcerative colitis (UC) is an inflammatory condition of the intestine, resulting from an increase in oxidative stress and pro-inflammatory mediators. In this study, the extract of endophytic bacterium *Rhizobium aegyptiacum* was prepared for the first time using liquid chromatography-mass spectrometry (LC-MS). In addition, also for the first time, the protective potential of *R. aegyptiacum* was revealed using an in vivo rat model of UC. The animals were grouped into four categories: normal control (group I), *R. aegyptiacum* (group II), acetic acid (AA)-induced UC (group III), and *R. aegyptiacum*-treated AA-induced UC (group IV). In group IV, *R. aegyptiacum* was administered at 0.2 mg/kg daily for one week before and two weeks after the induction of UC. After sacrificing the rats on the last day of the experiment, colon tissues were collected and subjected to histological, immunohistochemical, and biochemical investigations. There was a remarkable improvement in the histological findings of the colon tissues in group IV, as revealed by hematoxylin and eosin (H&E) staining, Masson's trichrome staining, and periodic acid-Schiff (PAS) staining. Normal mucosal surfaces covered with a straight, intact, and thin brush border were revealed. Goblet cells appeared magenta in color, and there was a significant decrease in the distribution of collagen fibers in the mucosa and submucosal connective tissues. All these findings were comparable to the respective characteristics of the control group. Regarding cyclooxygenase-2 (COX-2) immunostaining, a weak immune reaction was shown in most cells. Moreover, the colon tissues were examined using a scanning electron microscope, which confirmed the results of histological assessment. A regular polygonal unit pattern was seen with crypt orifices of different sizes and numerous goblet cells. Furthermore, the levels of catalase (CAT), myeloperoxidase (MPO), nitric oxide (NO), interleukin-6 (IL-6), and interlukin-1β (IL-1β) were determined in the colonic tissues of the different groups using colorimetric assay and enzyme-linked immunosorbent assay (ELISA). In comparison with group III, group IV exhibited a significant rise (P<0.05) in the CAT level but a substantial decline (P<0.05) in the NO, MPO, and inflammatory cytokine (IL-6 and IL-1β) levels. Based on reverse transcription-quantitative polymerase chain reaction (RT-qPCR), the tumor necrosis factor-α (*TNF-α*) gene expression was upregulated in group III, which was significantly downregulated (P<0.05) by treatment with *R. aegyptiacum* in group IV. On the contrary, the heme oxygenase-1 (*HO-1*) gene was substantially upregulated in group IV. Our findings imply that the oral consumption of *R. aegyptiacum* ameliorates AA-induced UC in rats by restoring and reestablishing the mucosal integrity, in addition to its anti-oxidant and anti-inflammatory effects. Accordingly, *R. aegyptiacum* is potentially effective and beneficial in human UC therapy, which needs to be further investigated in future work.

Key words: Inflammatory bowel syndrome; Liquid chromatography-tandem mass spectrometry (LC-MS/MS); Scanning electron microscopy (SEM); Histology; Immunohistochemistry; Reverse transcription-quantitative polymerase chain reaction (RT-qPCR)

✉ Engy ELEKHNAWY, engy.ali@pharm.tanta.edu.eg
Walaa A. NEGM, walaa.negm@pharm.tanta.edu.eg
* The two authors contributed equally to this work
Engy ELEKHNAWY, https://orcid.org/0000-0001-8287-1026
Walaa A. NEGM, https://orcid.org/0000-0003-0463-8047

Received Oct. 27, 2023; Revision accepted Feb. 20, 2024;
Crosschecked Jan. 20, 2025; Published online Jan. 25, 2025

1 Introduction

Most young adults without a gender preponderance suffer from ulcerative colitis (UC), a chronic inflammatory illness with no known etiology. The prevalence of UC is increasing globally and is greater in

industrialized countries (Ben-Horin et al., 2022). The definitive feature of UC is mucosal inflammation that begins in the rectum and spreads to the proximal portions of the colon. Clinically, UC typically manifests as persistent and bloody diarrhea. About a third of individuals experience extraintestinal symptoms, such as peripheral arthritis, primary sclerosing cholangitis, and pyoderma gangrenosum (Vavricka et al., 2011; Dignass et al., 2012).

Inflammation is central to the progress of various complex ailments like autoimmune illnesses and metabolic syndromes, with prostaglandins playing a major regulatory role. Cyclooxygenases such as cyclooxygenase-2 (COX-2) mediate inflammation via catalyzing arachidonic acid metabolism and in turn synthesizing prostaglandins (le Loupp et al., 2015).

Furthermore, when inducible nitric oxide synthase (iNOS) is activated, free radicals are triggered, which hinders the anti-oxidative system and thus could augment the damage to the intestinal mucosa (Wang and DuBois, 2010; Piechota-Polanczyk and Fichna, 2014). In addition, the excessive production of reactive oxygen species (ROS) could have a negative impact on the mucosal defense system (Checa and Aran, 2020).

The extended release of pro-inflammatory cytokines, like tumor necrosis factor-α (TNF-α), interleukin-6 (IL-6), and interleukin-1β (IL-1β), could trigger apoptosis, which possesses a central role in inflammatory bowel diseases (IBDs) like UC. It has been documented that apoptosis is integral to the pathophysiology of IBD (Gautam et al., 2013; Liu et al., 2022). This is attributed to the induction of apoptosis by the inflammatory process, which alters the function of the mucosal barrier and disturbs gut integrity (Raish et al., 2021).

The histological analysis of biopsy samples is essential for making a definite diagnosis, estimating the level of disease activity, assessing the likelihood of healing, and assessing the risk of relapse. Besides, histology is crucial for determining the treatment efficacy and identifying the side effects of treatment and long-standing UC, such as dysplasia (Adamina et al., 2021).

The current anti-inflammatory therapeutics for UC treatment suffers from many side effects like diarrhea, allergic responses, lymphopenia, vomiting, and elevation of the liver enzyme levels (Bruscoli et al., 2021). Therefore, it is critical to find novel therapeutics that could hinder the inflammatory cascade associated with the pathological consequences of UC.

Endophytic bacteria have the potential to enhance the growth and yield of plants and serve as biocontrol agents (Rana et al., 2020). They respond to biotic and abiotic hazards by enhancing biological N_2-fixation, producing phytohormone-soluble phosphate, inhibiting ethylene (C_2H_2) biosynthesis, and exhibiting bio-control action (Singh et al., 2017). Additionally, they can control the synthesis of secondary metabolites with significant therapeutic effects and exert a variety of biological effects (Twaij and Hasan, 2022).

Natural compounds represent a vital source for many bioactive therapeutics toward different ailments. Many researchers have investigated the potential therapeutic benefits of various plant and microbe metabolites against UC (Fan et al., 2020; Khare et al., 2020; Xue et al., 2023). To our knowledge, it is the first time that the endophytic bacterium *Rhizobium aegyptiacum* has been chemically analyzed using liquid chromatography-mass spectrometry (LC-MS), and its therapeutic potential on UC has been investigated in an animal model.

2 Materials and methods

2.1 Chemicals and drugs

All chemicals and solvents used were obtained from Sigma (USA), and culture media were obtained from Oxoid (UK).

2.2 Isolation of *R. aegyptiacum* endophytic bacteria

Healthy leaves of *Acalypha hispida* Burm. f. were harvested in summer from the plantation of the Faculty of Pharmacy, Tanta University, Egypt. The plant material was identified by Dr. Esraa AMMAR (Faculty of Science, Tanta University). After rinsing, the surface of *Acalypha* leaves was sterilized with 70% (volume fraction) ethyl alcohol for 2 min until drying. Subsequently, they were cut aseptically into small sections and imprinted onto yeast extract mannitol agar (YEMA) with incubation for 72 h at 28 °C in the dark. Finally, pure strains of *R. aegyptiacum* were obtained.

2.3 Identification of the endophytic bacteria

After the extraction of total DNA from the endophytic bacteria using a DNA extraction kit (Qiagen, Germany), the bacterial universal 16S ribosomal RNA (rRNA) gene was employed to characterize the isolated

strain. The forward and reverse primers were 5'-AGAG TTTGATCCTGGCTCAG-3' and 5'-GGTTACCTTGT TACGACTT-3', respectively (Lane, 1991). We determined the amplified gene sequences using ABI PRISM® 3100 Genetic Analyzer (Applied Biosystems, Thermo Fisher Scientific, USA). Finally, the obtained sequences were deposited in GenBank (https://blast.ncbi.nlm.nih.gov/Blast.cgi). The sequence homology was detected using the Basic Local Alignment Search Tool (BLAST). The phylogenetic tree was obtained using ClustalW software analysis (https://www.clustal.org).

2.4 Cultivation of *R. aegyptiacum*

The culture was prepared by first inoculating the endophytic bacterium *R. aegyptiacum* under sterile conditions into an Erlenmeyer conical flask with cotton plugs, which had been previously autoclaved and contained 500 mL yeast mannitol broth (10 flasks, 1 L each), and then incubating at 28 °C for 72 h in the dark.

2.5 LC-MS/MS

The LC-tandem MS (LC-MS/MS) analysis of the prepared endophytic bacterium *R. aegyptiacum* extract was performed according to previously reported methods (Attallah et al., 2022b; Elmongy et al., 2022). Details are shown in supplementary materials and methods.

2.6 Acetic acid (AA)-induced UC experiment

2.6.1 Animals

Forty male albino rats weighing approximately 210 g and aged 8–10 weeks were utilized, which were kept under standard conditions.

2.6.2 Induction of UC

UC was induced as previously described (Ansari et al., 2021). Details are shown in supplementary materials and methods.

2.6.3 Experimental design

The rats were allocated into four groups (n=10 each) as follows: (1) the rats received saline by oral gavage for three weeks and were administered 2 mL of saline in a single dose into the colon through a rubber catheter on the seventh day (group I, control group); (2) over the course of three weeks, the rats were given *R. aegypticaum* by oral gavage at a dosage of 0.2 mg/kg solution dissolved in carboxymethyl cellulose (group II, *R. aegyptiacum* group); (3) the same as the untreated group but with AA-induced colitis (group III, AA-induced UC group); (4) AA-induced colitis with the concomitant administration of *R. aegyptiacum* by oral gavage at 0.2 mg/kg daily for one week before and two weeks after the induction of colitis (group IV, *R. aegyptiacum*-treated AA-induced UC group).

2.6.4 Histological and immunohistochemical analyses

Distal colon samples from all studied groups were embedded in paraffin blocks after fixation in formalin. A routine histological examination of 5–6 μm thick slices was performed by staining with hematoxylin and eosin (H&E) (Bancroft and Gamble, 2008). Periodic acid-Schiff (PAS) reagent was used to detect goblet cells and the brush border of surface epithelium, and Masson trichrome stain was employed to detect the collagen fibers of connective tissue (Hsiao et al., 2021; Alherz et al., 2022). Morphometric analyses of the mean number of goblet cells and the mean area percentage of collagen fibers were conducted using ten non-overlapping readings obtained for each slide in all groups via image analysis tools (ImageJ). For immunohistochemical analysis, the colonic sections were deparaffinized, rehydrated, and incubated overnight at 4 °C with rabbit monoclonal COX-2 antibody (EPR12012, 1/250, ab179800, Abcam).

2.6.5 Scanning electron microscopy (SEM)

Colonic tissues were examined using SEM. Details are shown in supplementary materials and methods.

2.6.6 Colorimetric evaluation and ELISA investigation

The catalase (CAT), myeloperoxidase (MPO), and nitric oxide (NO) levels were evaluated in colon homogenates by CAT, MPO, and NO assay kits, respectively (Abcam, USA).

The IL-6 and IL-10 levels were determined in the colon tissue homogenates using enzyme-linked immunosorbent assay (ELISA) kits (Sun Red Biotechnology Co., China) and the results were read by an ELISA microplate reader at 450 nm.

2.6.7 Reverse transcription-quantitative polymerase chain reaction (RT-qPCR)

After the extraction of total RNA by TRIzols (Life Technologies, USA) (Livak and Schmittgen, 2001), it was converted to complementary DNA (cDNA) by the

QuantiTect kit (Qiagen, USA). Then, cDNA was amplified by the Maxima SYBR Green Master Mix (Thermo Fisher Scientific, USA). The employed primers (β-actin, heme oxygenase-1 (*HO-1*), and *TNF-α*) are documented in Table S1 (Mi et al., 2017).

2.7 Statistical analysis

The analysis of variance (ANOVA) was performed to detect significant differences among the studied groups. The results were expressed as mean±standard deviation (SD) using Graph Pad Prism software (USA), and the statistical significance was determined at $P<0.05$.

3 Results

3.1 Identification of the isolated endophytic bacteria

The bacterial isolate was identified as *R. aegyptiacum* (accession number: ON100826), which has the identity of 99.93% with its highly similar isolate *R. aegyptiacum* strain 1010 16S rRNA, partial sequence (accession number: NR_137399.1) (Fig. S1).

3.2 Phytochemical profiling

A total of 31 compounds were tentatively identified in the *R. aegyptiacum* extract using both the positive and negative modes of LC-electrospray ionization (ESI)-MS/MS. The main components were several types of amino acids, flavonoids, coumarins, and other glycosylated compounds. The obtained metabolite profile is presented in Table 1 and Figs. S2 and S3. The mass/mass spectra shown in Figs. 1 and 2 display the fragmentation pattern of the most abundant detected metabolites in positive and negative modes.

3.3 H&E staining

The H&E-stained colonic tissues of groups I and II revealed a normal mucosal surface covered with a thin striated brush border. The mucosal lamina propria contained simple tubular intestinal glands (crypts of

Table 1 Phytochemical profiling of *Rhizobium aegyptiacum* extract using LC-ESI-MS/MS different modes

No.	RT (min)	Precursor, *m/z*	Error (ppm)	Name	Formula	Adduction	MS/MS spectrum, *m/z*	Class
1	0.97	191.0201	−0.6	Citric acid	$C_6H_8O_7$	$[M-H]^-$	173.0089, 129.0194, 87.0089, 57.0347	Tricarboxylic acids and derivatives
2	1.05	117.0185	0	Succinic acid	$C_4H_6O_4$	$[M-H]^-$	117.0191, 99.0074, 73.0296, 55.0187	Dicarboxylic acids and derivatives
3	1.05	161.0441	−2.5	3-Hydroxy-3-methylglutaric acid	$C_6H_{10}O_5$	$[M-H]^-$	101.2130, 99.0452, 59.0151, 57.0341	Hydroxy fatty acids
4	1.07	133.0136	−0.9	Malic acid	$C_4H_6O_5$	$[M-H]^-$	115.0042, 89.0272, 87.0099, 72.9937, 71.0143	Beta hydroxy acids and derivatives
5	1.15	104.1069	−5.4	Choline	$C_5H_{14}NO$	$[M]^+$	60.0814, 58.0657	Cholines
6	1.16	195.0520	0.8	Gluconic acid	$C_6H_{12}O_7$	$[M-H]^-$	177.0394, 160.8413, 75.0089, 59.0141	Medium-chain hydroxy acids and derivatives
7	1.17	162.1123	−0.7	Carnitine	$C_7H_{15}NO_3$	$[M+H]^+$	103.0386, 102.0902, 85.0284, 60.0805	Carnitines
8	1.20	144.0685	0.6	4-Acetamidobutanoic acid	$C_6H_{11}NO_3$	$[M-H]^-$	102.0563, 100.0782, 58.0302, 54.0352	γ-Amino acids and derivatives
9	1.25	175.0582	−0.8	L-Arginine	$C_6H_{14}N_4O_2$	$[M+H]^+$	158.0902, 116.0687, 70.0648, 60.0542	L-α-Amino acids
10	1.25	146.1192	0.9	Deoxycarnitine	$C_7H_{15}NO_2$	$[M+H]^+$	87.0442, 60.0820, 58.0663	Straight chain fatty acids
11	1.27	118.0866	−2.3	Glycine-betaine	$C_5H_{11}NO_2$	$[M+H]^+$	59.0723, 58.0642	α-Amino acids
12	1.29	181.0722	0.1	Mannitol	$C_6H_{14}O_6$	$[M-H]^-$	163.0617, 101.0243, 89.0245, 59.0142	Sugar alcohols
13	1.32	341.1127	0.9	Palatinose	$C_{12}H_{22}O_{11}$	$[M-H]^-$	222.0667, 179.0563, 119.0351, 89.0242	*O*-Glycosyl compounds

To be continued

Table 1 (continued)

No.	RT (min)	Precursor, *m/z*	Error (ppm)	Name	Formula	Adduction	MS/MS spectrum, *m/z*	Class
14	1.76	130.0497	0.3	L-5-Oxoproline	$C_5H_7NO_3$	$[M+H]^+$	84.0439, 56.0491	α-Amino acids and derivatives
15	2.04	164.0707	0.3	Phenylalanine	$C_9H_{11}NO_2$	$[M-H]^-$	147.0457, 103.0561, 91.0566, 72.0093	Phenylalanines and derivatives
16	2.10	162.0780	0.8	*O*-Acetyl-L-homoserine	$C_6H_{11}NO_4$	$[M+H]^+$	127.0396, 120.0660, 102.0553	L-α-Amino acids
17	2.15	166.0863	0	Phenylalanine	$C_9H_{11}NO_2$	$[M+H]^+$	120.0809, 103.0567, 77.0380	Phenylalanines and derivatives
18	6.03	211.1445	−0.4	3-Butan-2-yl-2,3,6,7,8,8a-hexahydropyrrolo[1,2-a]pyrazine-1,4-dione	$C_{11}H_{18}N_2O_2$	$[M+H]^+$	183.1529, 154.0747, 138.1287, 70.0645	α-Amino acids and derivatives
19	6.75	209.0810	0.7	3,4-Dimethoxy cinnamic acid	$C_{11}H_{12}O_4$	$[M+H]^+$	191.0711, 165.0715, 135.0810, 107.0856	Coumaric acids and derivatives
20	8.43	285.0393	0.4	Luteolin	$C_{15}H_{10}O_6$	$[M-H]^-$	268.0384, 257.0463, 241.0507	Flavones
21	8.60	227.0912	0.8	2-Hydroxyjasmonic acid	$C_{12}H_{18}O_4$	$[M+H]^+$	191.0674, 149.0944, 131.0860, 107.0820	Jasmonic acids
22	8.76	254.1394	0.2	*N*-[1-(4-Methoxy-6-oxopyran-2-yl)-2-methylbutyl] acetamide	$C_{13}H_{19}NO_4$	$[M+H]^+$	212.1278, 156.0659, 125.0234	Pyranones and derivatives
23	8.82	245.1367	−0.9	8-Hydroxy-3-methoxycarbonyl-2-methylidenenonanoic acid	$C_{12}H_{20}O_5$	$[M+H]^+$	177.0915, 149.0961, 131.0852, 79.0540	Medium-chain hydroxy acids and derivatives
24	9.21	434.1786	−0.6	(3Z)-6-Hydroxy-3-(1H-imidazol-5-ylmethylene)-12-methoxy-7a-(2-methyl-3-buten-2-yl)-7a,12-dihydro-1H,5H-imidazo[1',2':1,2]pyrido[2,3-b]indole-2,5(3H)-dione	$C_{23}H_{23}N_5O_4$	$[M+H]^+$	403.1638, 334.0912, 289.0704, 261.0754	Pyridoindolones
25	9.52	299.0548	0.9	Kaempferide	$C_{16}H_{12}O_6$	$[M-H]^-$	284.0270, 255.0664, 151.0023	Flavonols
26	9.80	237.0789	−0.5	5,6,7-Trimethoxychromen-2-one	$C_{12}H_{12}O_5$	$[M+H]^+$	222.0513, 207.0274, 179.0326	Coumarins and derivatives
27	12.59	432.1649	0	(3Z)-6-Hydroxy-3-(1H-imidazol-5-ylmethylene)-12-methoxy-7a-(2-methyl-3-buten-2-yl)-7a,12-dihydro-1H,5H-imidazo[1',2':1,2]pyrido[2,3-b]indole-2,5(3H)-dione	$C_{23}H_{23}N_5O_4$	$[M-H]^-$	332.0771, 304.0831, 276.0894, 177.0417	Pyridoindolones
28	13.18	343.2918	−0.4	Cocamidoprpyl betaine	$C_{19}H_{38}N_2O_3$	$[M+H]^+$	240.2325, 183.1727, 57.0690	α-Amino acids
29	16.26	639.1719	−0.9	Secalonic acid	$C_{32}H_{30}O_{14}$	$[M+H]^+$	621.1589, 589.1319, 579.1508, 561.1398	Xanthones
30	18.09	277.2157	−1.0	Linolenic acid	$C_{18}H_{30}O_2$	$[M-H]^-$	233.1540, 208.9221	Lineolic acids and derivatives
31	23.22	281.2488	0.8	Elaidic acid	$C_{18}H_{34}O_2$	$[M-H]^-$	281.2472, 263.2372	Long-chain fatty acids

LC-ESI-MS/MS: liquid chromatography-electrospray ionization-tandem mass spectrometry; RT: retention time; *m/z*: mass-to-charge ratio; ppm: 10^{-6}.

Spectrum from IDA-NEG-221009-CM0019-1.wiff (sample 1)–IDA-NEG-221009-CM0019-1, Experiment 6, −TOF MS² (50–1000) from 0.973 min
Precursor: 191.0 Da CE=−35

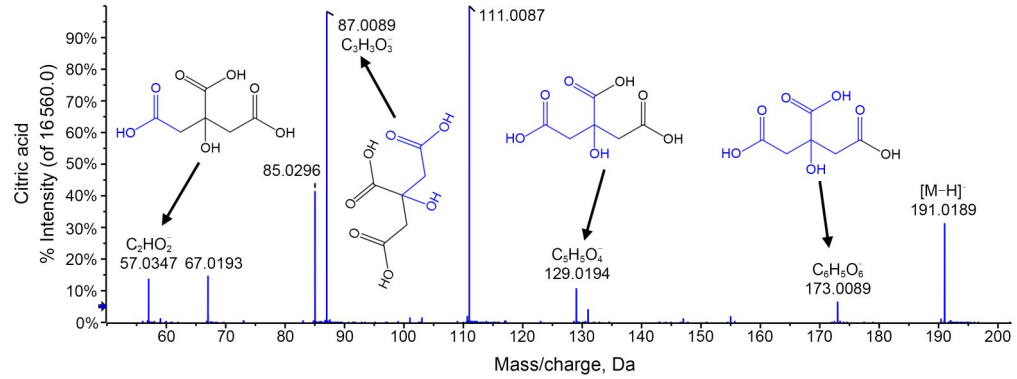

Spectrum from IDA-NEG-221009-CM0019-1.wiff (sample 1)–IDA-NEG-221009-CM0019-1, Experiment 6, −TOF MS² (50–1000) from 1.279 min
Precursor: 181.1 Da CE=−35

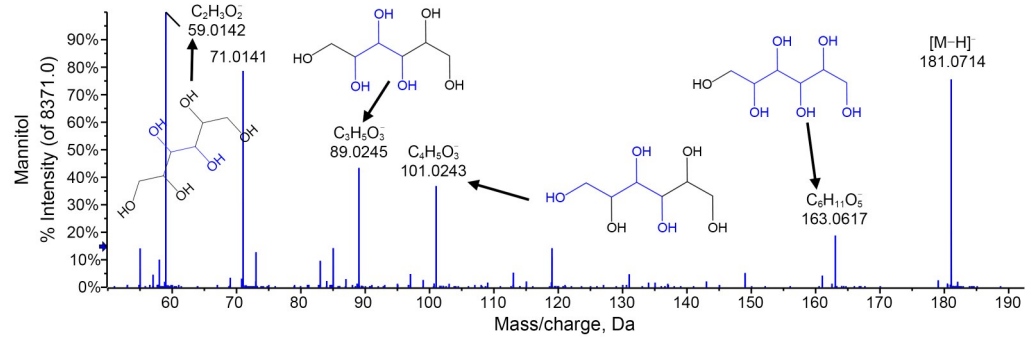

Spectrum from IDA-NEG-221009-CM0019-1.wiff (sample 1)–IDA-NEG-221009-CM0019-1, Experiment 2, −TOF MS² (50–1000) from 23.223 min
Precursor: 281.2 Da CE=−35

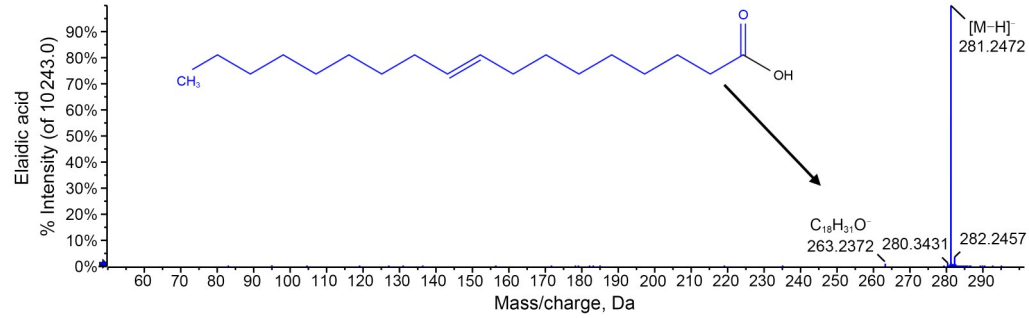

Spectrum from IDA-NEG-221009-CM0019-1.wiff (sample 1)–IDA-NEG-221009-CM0019-1, Experiment 3, −TOF MS² (50–1000) from 1.163 min
Precursor: 195.1 Da CE=−35

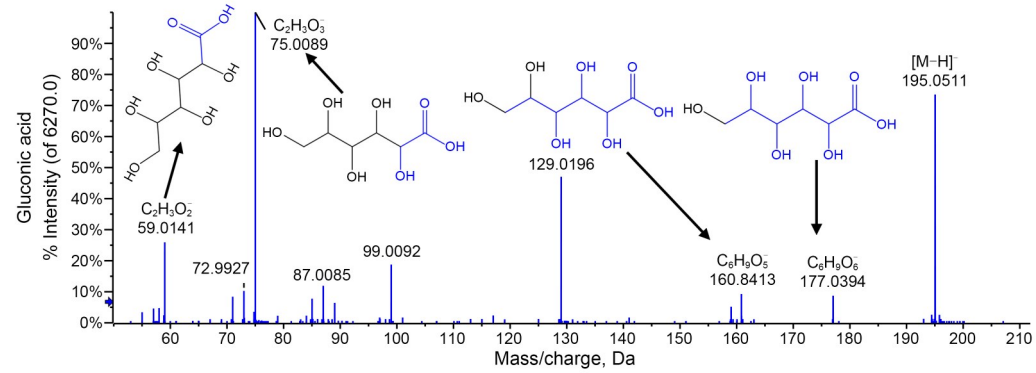

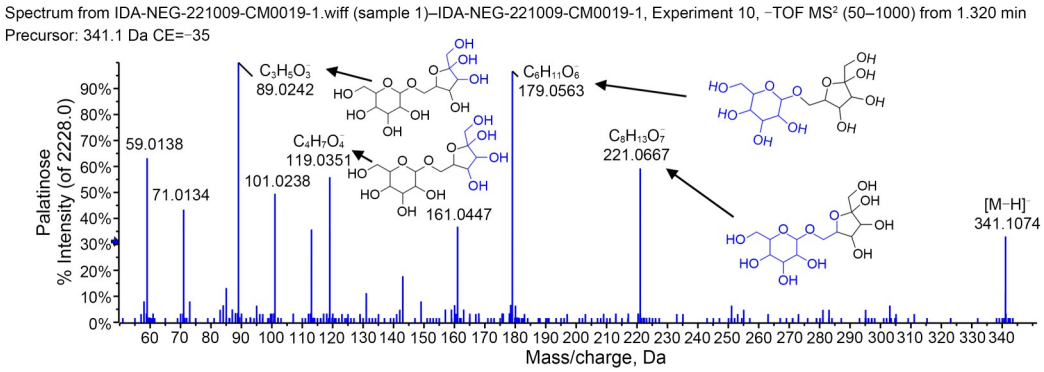

Fig. 1 Most abundant compounds detected in negative liquid chromatograph-mass spectrometer (LC-MS) mode.

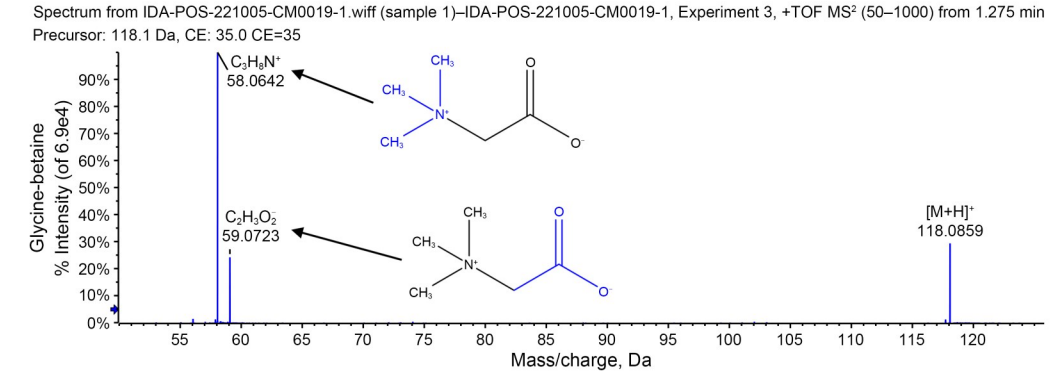

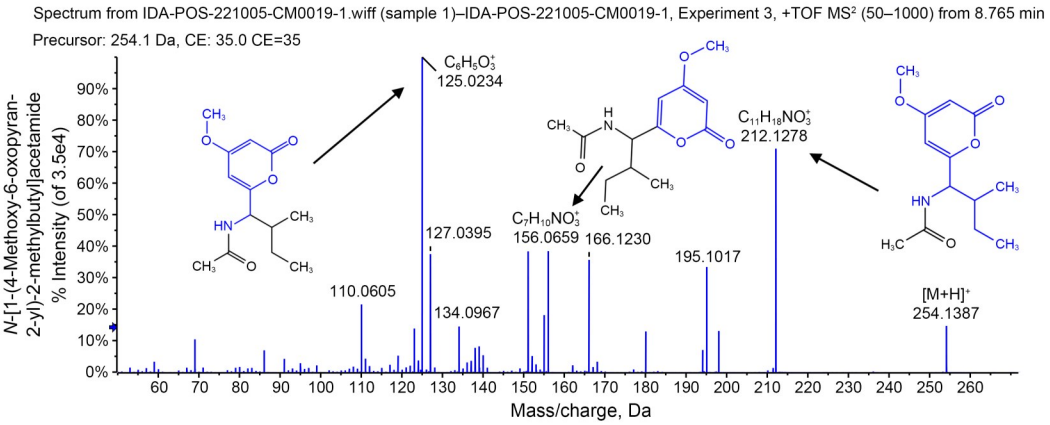

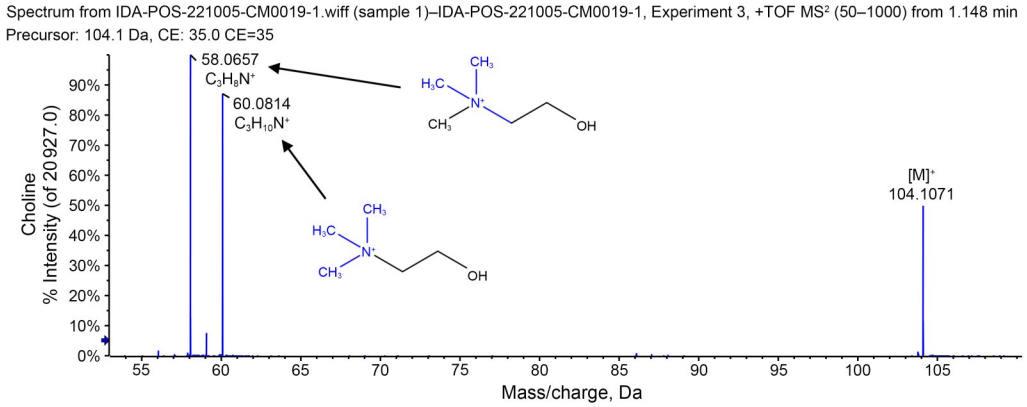

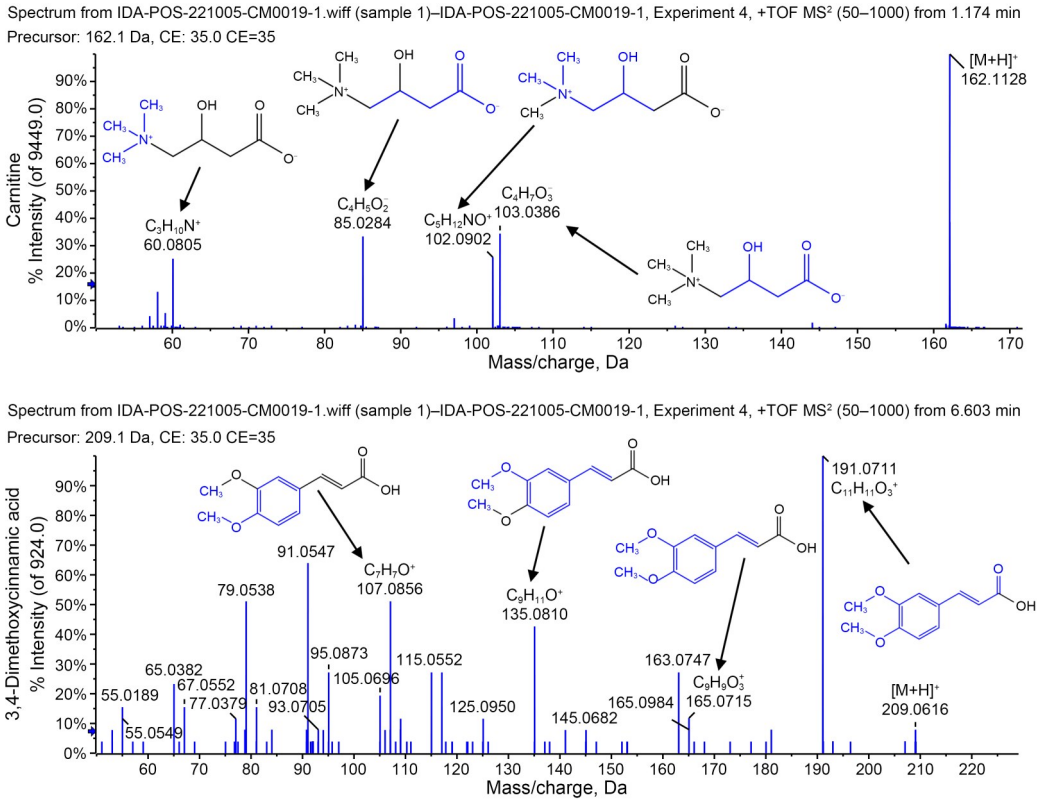

Fig. 2 Most abundant compounds detected in positive liquid chromatograph-mass spectrometer (LC-MS) mode.

Lieberkühn). The crypts were long, deep, and straight, and were lined with numerous goblet cells. Mononuclear cells could be observed to fill the space between glands in the lamina propria (Figs. 3a–3d). On the other hand, in group III with AA-induced colitis, structural changes of the mucosal and epithelial abnormalities were revealed, including focal loss of surface epithelium and part of the lamina propria with widespread architectural crypt distortion and increased cellularity of the lamina propria in the form of disseminated inflammatory cellular infiltration in the glandular tissue (Figs. 3e and 3f). Also, there was an apparent reduction in the number of goblet cells with crypt cyst and abscess formation. Meanwhile, the concomitant administration of *R. aegyptiacum* with AA in group IV revealed a histological image resembling that of the control group. However, there were focal inflammatory cellular infiltration and widening of the submucosa (Figs. 3g and 3h).

3.4 Staining with PAS reagent

The analysis of PAS-stained colonic sections of both groups I and II exhibited intact PAS-positive thin brush borders of columnar cells. In contrast, goblet cells were detected in the epithelium with the characteristic magenta color of mucin secretion (Figs. 4a and 4b). Meanwhile, group III showed an evident statistically significant reduction in goblet cells and an interrupted brush border (Fig. 4c). On the other hand, group IV exhibited a straight, intact, and thin brush border, and goblet cells appeared magenta in color without statistically significant differences compared to the control group (Figs. 4d and 4e).

3.5 Masson's trichrome staining

The examination of Masson's trichrome-stained colonic sections of both groups I and II revealed the arrangement and distribution of collagen fibers in the lamina propria between the tubular glands and submucosal connective tissue (Figs. 5a−5d). In contrast, group III exhibited a statistically significant increase in the distribution of collagen fibers in the mucosal and submucosal connective tissues (Figs. 5e and 5f). Meanwhile, group IV showed a statistically significant decrease in the distribution of collagen fibers in the mucosal and submucosal connective tissues in comparison to group III,

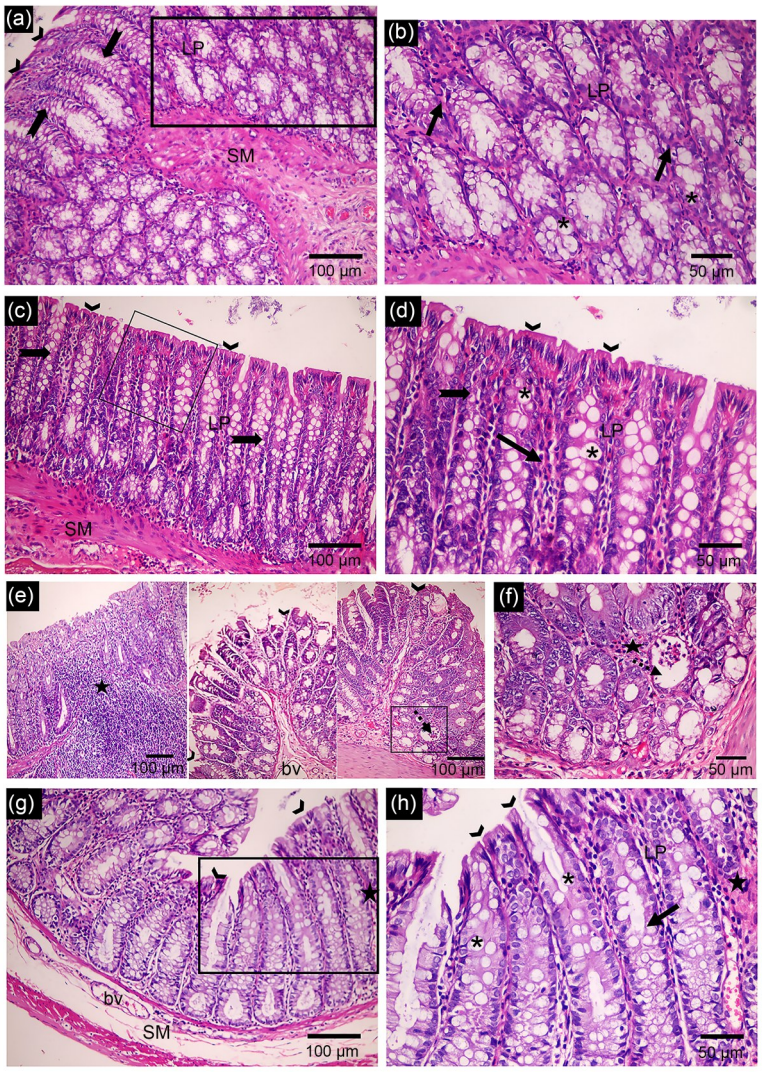

Fig. 3 Light microscope images of the distal colon sections of adult male albino rats in all studied groups by hematoxylin and eosin (H&E) staining. The images b, d, f, and h represent higher magnifications of selected square areas of the images a, c, e, and g, respectively. (a–d) Groups I and II show normal colonic mucosa and submucosa (SM). The mucosal surface is covered with a thin striated brush border (arrowheads). The mucosal lamina propria (LP) contains simple tubular intestinal glands (crypts of Lieberkühn). The crypts are long, deep, and straight (bifid arrows), and are lined by numerous goblet cells (asterisks). Mononuclear cells fill the space between glands in the lamina propria (arrows). (e, f) Group III with acetic acid (AA)-induced colitis shows focal loss of surface epithelium and part of the lamina propria (arrowheads) with inflammatory cellular infiltration in the glandular tissue (star). Furthermore, there is an apparent reduction in the number of goblet cells and crypt cyst formation (dashed arrow). (g, h) Group IV shows a normal histological image of the colonic mucosa with a straight intact brush border (arrowheads) and numerous goblet cells in the glandular tissue (asterisks). However, focal inflammatory cell infiltration (star) and widening of the SM exist. bv: blood vessel. H&E ×200, scale bar=100 μm; H&E ×400, scale bar=50 μm.

with no statistically significant difference relative to the control group (Figs. 5g–5i).

3.6 Immunohistochemical study of COX-2-stained sections

The colonic tissues in group III (AA-induced UC) rats had strong positive COX-2 immunoreactivity, with a statistically significant increase in the area percentage of COX-2-positive immunostaining relative to both groups I and II. At the same time, group IV showed a weak positive reaction without a statistically significant difference compared to the control group, and a statistically significant decrease in the area percentage of COX-2-positive immunostaining relative to group III (Fig. 6).

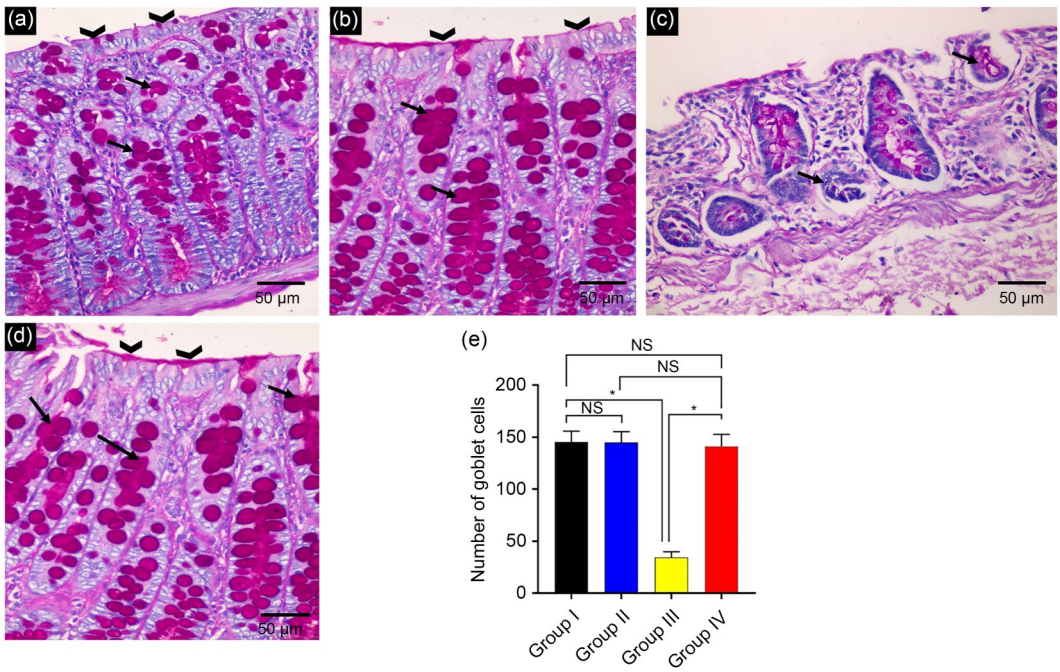

Fig. 4 Sections of the distal colon of adult male albino rats in all studied groups by periodic acid-Schiff (PAS) staining. (a, b) The control (a) and rhizobium (b) groups showing a PAS-positive thin brush border (arrowheads) and goblet cells colored magenta (arrows). (c) The acetic acid (AA) group presenting a reduction in the number of goblet cells (arrows) with the interruption of the brush border. (d) The rhizobium+AA group showing a thin brush border without interruption (arrowheads) and goblet cells (arrows) positively stained with magenta-colored mucin secreted from the cells. (e) The number of goblet cells in all studied groups. The data are expressed as mean±standard deviation (SD), n=10. NS means no significant difference and the single asterisk represents significant difference (P<0.05). PAS ×400, scale bar=50 μm.

3.7 SEM

SEM examination of the colonic epithelium in groups I and II revealed a regular pattern of polygonal units with regular size separated by deep gutters. The epithelium invaginated to form many crypts, and numerous goblet cells could be seen (Figs. 7a–7c). Group III samples exhibited enlarged crypt orifices, ulceration of surface epithelium, and disorganization of polygonal units. In addition, few goblet cells were recognized (Figs. 7d–7f). Group IV (*R. aegyptiacum*+AA) demonstrated a regular polygonal unit pattern with crypt orifices of different sizes and numerous goblet cells similar to those of the control group (Figs. 7g and 7h).

3.8 Colorimetric studies

In group IV, a significant rise (P<0.05) in the CAT level was revealed in comparison with group III (Fig. 8a). On the other hand, group IV showed a substantial decline (P<0.05) in NO and MPO levels (Figs. 8b and 8c).

3.9 ELISA analyses

Group IV samples presented a substantial decline (P<0.05) in the levels of inflammatory cytokines IL-6 and IL-1β in comparison with group III (Fig. 9).

3.10 RT-qPCR studies

We observed an upregulation of the *TNF-α* gene expression in group III, which was significantly downregulated (P<0.05) by treatment with *R. aegyptiacum* in group IV. On the other hand, a substantial upregulation of the *HO-1* gene was revealed in group IV (Fig. 10).

4 Discussion

Plants can have associations with different members of the ecosystem living in the surrounding environment (Almukainzi et al., 2022). Microorganisms, especially bacteria, are vital for their beneficial associations with various plants (Abdelaziz et al., 2019). These bacteria form mutualistic interactions with several

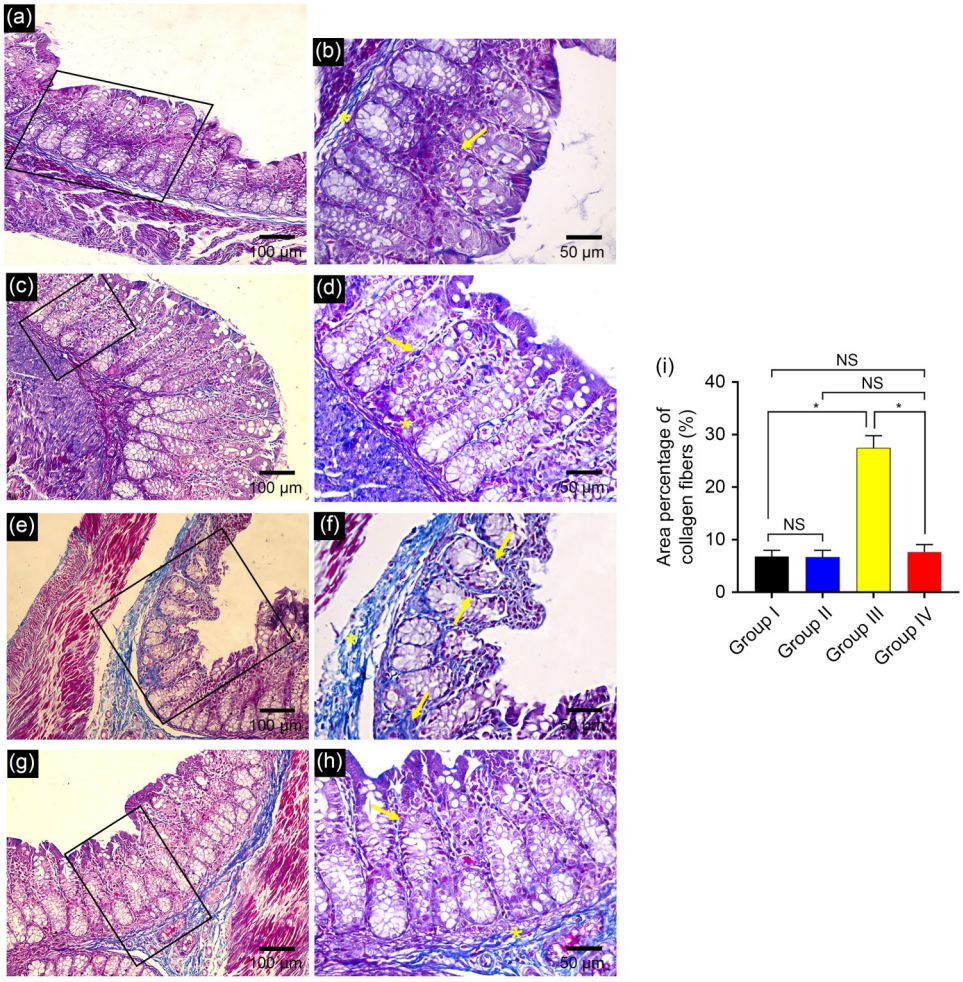

Fig. 5 Sections of the distal colon of adult male albino rats in all studied groups by Masson's trichrome staining. Collagen fibers in the mucosa (arrows) and in the submucosa (asterisks). The images b, d, f, and h represent higher magnifications of selected square areas of the images a, c, e, and g, respectively. (a–d) The control and rhizobium groups showing the arrangement of collagen fibers in the lamina propria between glands and in the submucosal connective tissue. (e, f) The acetic acid (AA) group showing an evident increase in collagen fibers in the mucosal and submucosal connective tissues. (g, h) The rhizobium+AA group exhibiting some collagen fibers in the mucosal and submucosal connective tissues. (i) The area percentage of collagen fibers in all studied groups. All data are expressed as mean±standard deviation (SD), *n*=10. NS means no significant difference and the single asterisk represents significant difference (*P*<0.05). Masson's trichrome staining ×200, scale bar=100 μm; Masson's trichrome staining ×400, scale bar=50 μm.

advantages to their host. One of these is assisting plants in withstanding different types of stresses that could hinder their growth (Elekhnawy and Negm, 2022). Several bioactive metabolites with pharmacological activities have been isolated from medicinal plant endophytes and structurally identified using various conventional and modern methods. These metabolites have given researchers a starting point to build upon as they continue to create and formulate bioactive molecules into effective medicines with wide-ranging applications in the health care system and many other facets of human existence (Quettier-Deleu et al., 2000; Attallah et al., 2022a). Endophytes are typically connected to the secondary metabolites and therapeutic properties of medicinal plants (Strobel and Daisy, 2003). To this end, the current study isolated an endophytic bacterial isolate from *A. hispida* leaves and identified it using 16S rRNA sequencing. Then, LC-MS/MS was performed to determine the bioactive components of the endophytic bacteria. The identified metabolites were found to belong to several phytochemical classes, including amino acids, flavonoids, coumarins, and other glycosylated compounds. The major detected metabolites in the negative mode were citric acid, elaidic acid, mannitol, gluconic

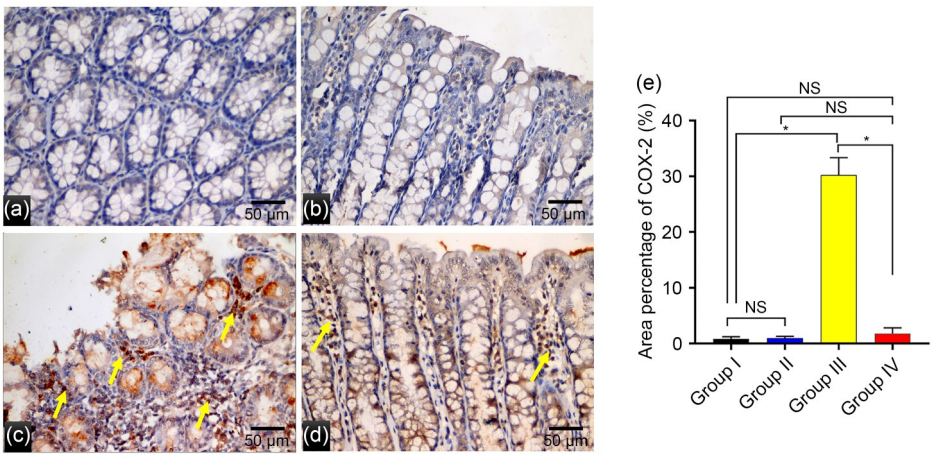

Fig. 6 Sections of the distal colon of adult male albino rats in different studied groups by cyclooxygenase-2 (COX-2) staining. (a) The control group with a negative COX-2 immune reaction in colonic cells. (b) The rhizobium group showing a negative expression of COX-2 immune reaction in all cells. (c) The acetic acid (AA) group presenting a strong positive immune reaction in surface epithelial and glandular cells (arrows). (d) The rhizobium+AA group with weak immune reaction in most cells (arrows). (e) The area percentage of COX-2 in all studied groups. All data are expressed as mean±standard deviation (SD), *n*=10. NS means no significant difference and the single asterisk represents significant difference (*P*<0.05). COX-2 immune reaction in the cells immunostaining ×400, scale bar=50 μm.

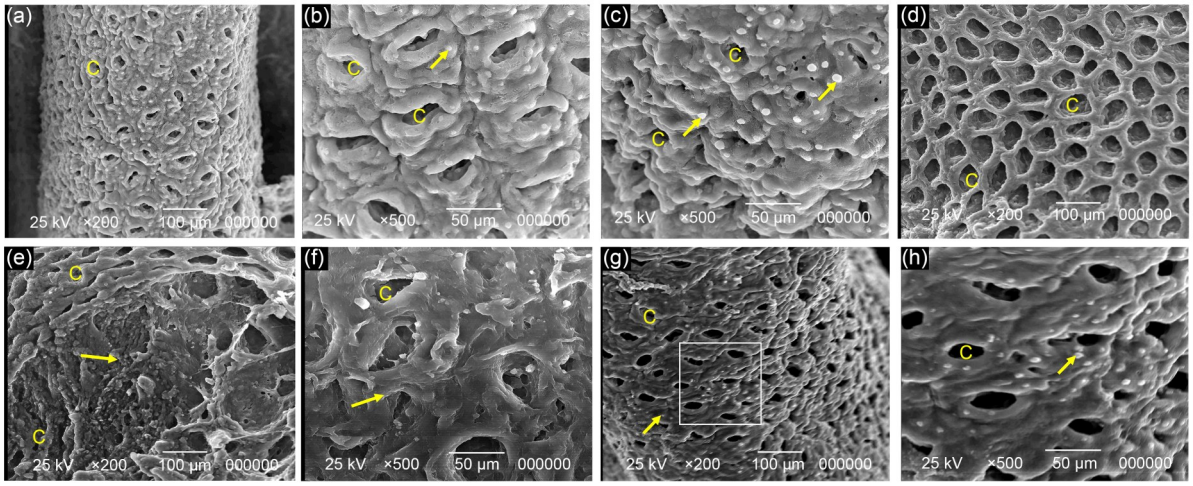

Fig. 7 Representative scanning electron microscopy (SEM) images of the distal colon in all studied groups. (a–c) Groups I and II show a regular pattern of polygonal units with regular size separated by deep gutters, with goblet cells (arrows) and the crypt opening (C). (d–f) The acetic acid (AA) group III shows enlarged crypt orifices (C) (d), ulceration of surface epithelium (arrows) (e), and disorganization of polygonal units. Few goblet cells are recognized. (g, h) Group IV (*R. aegyptiacum*+AA) presents a regular polygonal unit pattern with crypt orifices (C) of different sizes and numerous goblet cells (arrows). The image h represents higher magnification of the selected square area of the image g. SEM ×200, scale bar=100 μm; SEM ×500, scale bar=50 μm.

acid, and palatinose, while those in the positive mode included glycine-betaine, *N*-[1-(4-methoxy-6-oxopyran-2-yl)-2-methylbutyl]acetamide, choline, carnitine, and 3,4-dimethoxy cinnamic acid.

The protective potential of the endophytic *R. aegyptiacum* against the AA-induced UC in rats was investigated for the first time. In the present study, the assessment with H&E staining revealed that, in the AA-induced colitis group, structural changes of mucosal and epithelial abnormalities were present, including focal loss of surface epithelium and disseminated inflammatory cellular infiltration, which were in accordance with a previous study (Bertevello et al., 2005). Ansari et al. (2021) indicated that the AA-induced colitis group stained with PAS displayed deceptively decreased goblet cells and reduced mucin score, which was also reported

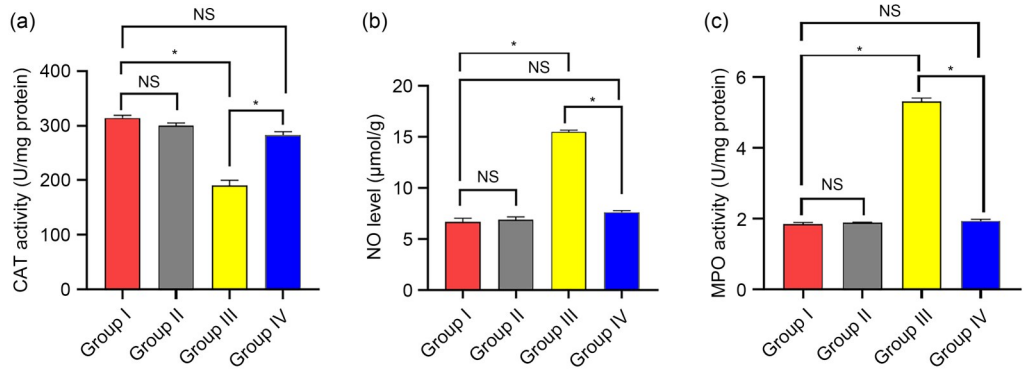

Fig. 8 Levels of catalase (CAT) (a), nitric oxide (NO) (b), and myeloperoxidase (MPO) (c) in the different experimental groups. All data are expressed as mean±standard deviation (SD), *n*=10. NS designates no significant difference (*P*>0.05) and the asterisk designates significant difference (*P*<0.05).

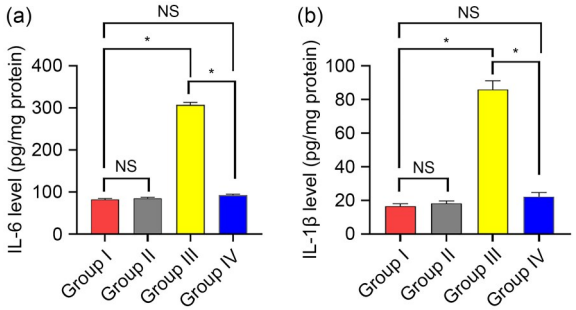

Fig. 9 Levels of interleukin-6 (IL-6) (a) and IL-1β (b) in the studied groups. All data are expressed as mean±standard deviation (SD), *n*=10. NS designates no significant difference (*P*>0.05) and the asterisk designates significant difference (*P*<0.05).

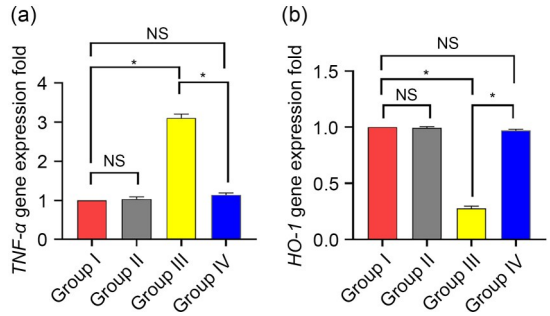

Fig. 10 Fold changes in tumor necrosis factor-α (*TNF-α*) (a) and heme oxygenase-1 (*HO-1*) (b) gene expression in different groups. All data are expressed as mean±standard deviation (SD), *n*=10. NS designates no significant difference (*P*>0.05) and the asterisk designates significant difference (*P*<0.05).

in the current study. The mucosal structure damage, inflammation, and reduction in goblet cells numbers were enhanced by the administration of *R. aegyptiacum*. COX-2 was expressed in mucosal epithelial cells in the AA-induced colitis group and this expression was significantly decreased by the administration of *R. aegyptiacum*. Endophytic metabolites had been suggested as a possible source of recent natural antioxidants. The endophytic fungus *Xylaria* sp. obtained from the leaves of ginkgo biloba exhibited antioxidant activity (Liu et al., 2007; Khairy et al., 2018).

The main pathophysiology of UC includes increases in oxidative stress and pro-inflammatory mediators like TNF-α, IL-6, and IL-1β. This was confirmed in the AA-induced UC group in the current study, in line with previous investigations (Ran et al., 2008; Li et al., 2020; Raish et al., 2021; Shahid et al., 2022). COX-2 produces prostaglandin E2 (PGE2), which in turn triggers intestinal edema and hyperemia (Abdallah et al., 2020; Alotaibi et al., 2022). Thus, the increase in COX-2, as revealed by the immunohistochemical investigations, along with the substantial increase in the MPO and NO, has resulted in augmentation of the inflammatory process and depletion of the anti-oxidative system (represented by CAT activity) in the colon tissues (Khairy et al., 2018). The administration of *R. aegyptiacum* markedly ameliorated all such pathological changes. Interestingly, certain identified compounds in the *R. aegyptiacum* extract had been documented to have anti-inflammatory and/or antioxidant potential; different studies have demonstrated the anti-inflammatory potential of the bacterial extract compounds. Peyrottes et al. (2020) reported that *O*-acetyl-L-homoserine decreased the IL-6 level in murine macrophage cell lines stimulated with lipopolysaccharide (LPS) and interferon-γ (IFN-γ). Wang et al. (2021) documented that leucine-proline-phenylalanine-derived peptide suppressed the messenger RNA (mRNA) expression of *iNOS*, *COX-2*, and *TNF-α* in LPS-irritated RAW264.7.

In addition, Aziz et al. (2018) proved the strong in vivo and in vitro anti-inflammatory activity of luteolin. The action mechanism of luteolin includes the nuclear factor-κB (NF-κB), mitogen-activated protein kinase (MAPK), and the signal transducer and activator of transcription 3 (STAT3) pathways.

Many previous studies have reported the beneficial impacts of other groups of bacteria (probiotics) in treating UC (Blacher et al., 2017; Popov et al., 2021). Probiotics like *Bifidobacterium* and *Lactobacillus* can improve intestinal barrier integrity, which is attained by metabolizing short-chain fatty acids, tryptophan, and other chemicals, leading to the increased production of mucin and tight junction proteins in the intestinal epithelial cells (Kaur et al., 2020; Lavelle and Sokol, 2020). Further evidence suggests the ability of probiotics to regulate intestinal immunity, preventing the excessive activation of the intestinal immune cells and reducing the levels of certain pro-inflammatory mediators, such as IL-6, TNF-α, and IL-1β. Moreover, it was proved that probiotics could increase the levels of anti-inflammatory factors, like IL-10 and transforming growth factor-β (TGF-β). This, along with inhibited expression of the NF-κB signaling pathway, could improve intestinal inflammation (Lavelle and Sokol, 2020). Overall, this study provides a basis for using certain groups of bacteria (endophytic bacteria) to treat UC.

5 Conclusions

Our investigation revealed that *R. aegyptiacum* as an endophytic bacterium can effectively restore the normal conditions of colonic mucosa after inducing ulcer through the administration of AA in UC rats. Most importantly, we demonstrated for the first time that *R. aegyptiacum* possesses antioxidant and anti-inflammatory properties. Future studies are required to endorse the clinical use of *R. aegyptiacum* in managing human UC patients.

Data availability statement

All data are available in the manuscript and the supporting materials.

Acknowledgments

Funding note: Open access funding provided by The Science, Technology & Innovation Funding Authority (STDF) in cooperation with The Egyptian Knowledge Bank (EKB).

Author contributions

Engy ELEKHNAWY, Duaa ELIWA, Sarah IBRAHIM, Asmaa Ramadan AZZAM, and Walaa A. NEGM performed the experimental research and data analysis, and wrote and edited the manuscript. Sebaey MAHGOUB, Sameh MAGDELDIN, Ehssan MOGLAD, and Rehab AHMED contributed to the study design, data analysis, writing and editing of the manuscript. All authors have read and approved the final manuscript, and therefore, have full access to all the data in the study and take responsibility for the integrity and security of the data.

Compliance with ethics guidelines

Engy ELEKHNAWY, Duaa ELIWA, Sebaey MAHGOUB, Sameh MAGDELDIN, Ehssan MOGLAD, Sarah IBRAHIM, Asmaa Ramadan AZZAM, Rehab AHMED, and Walaa A. NEGM declare that they have no conflict of interest.

All procedures followed were in accordance with the ethical standards of the responsible committee on animal experimentation (Medical Research Ethics Committee, Faculty of Medicine, Tanta University, Egypt, with an approval number 36264PR357/9/23).

References

Abdallah HMI, Ammar NM, Abdelhameed MF, et al., 2020. Protective mechanism of *Acacia saligna* butanol extract and its nano-formulations against ulcerative colitis in rats as revealed via biochemical and metabolomic assays. *Biology (Basel)*, 9(8):195. https://doi.org/10.3390/biology9080195

Abdelaziz A, Sonbol F, Elbanna T, et al., 2019. Exposure to sublethal concentrations of benzalkonium chloride induces antimicrobial resistance and cellular changes in *Klebsiellae pneumoniae* clinical isolates. *Microb Drug Resist*, 25(5): 631-638. https://doi.org/10.1089/mdr.2018.0235

Adamina M, Feakins R, Iacucci M, et al., 2021. ECCO topical review optimising reporting in surgery, endoscopy, and histopathology: collaboration between S-ECCO, EduCom, H-ECCO. *J Crohns Colitis*, 15(7):1089-1105. https://doi.org/10.1093/ecco-jcc/jjab011

Alherz FA, Negm WA, Elekhnawy E, et al., 2022. Silver nanoparticles prepared using *Encephalartos laurentianus* De Wild leaf extract have inhibitory activity against *Candida albicans* clinical isolates. *J Fungi (Basel)*, 8(10):1005. https://doi.org/10.3390/jof8101005

Almukainzi M, El-Masry TA, Negm WA, et al., 2022. Co-delivery

of gentiopicroside and thymoquinone using electrospun m-PEG/PVP nanofibers: in-vitro and in vivo studies for antibacterial wound dressing in diabetic rats. *Int J Pharm*, 625:122106. https://doi.org/10.1016/j.ijpharm.2022.122106

Alotaibi B, El-Masry TA, Elekhnawy E, et al., 2022. Aqueous core epigallocatechin gallate PLGA nanocapsules: characterization, antibacterial activity against uropathogens, and *in vivo* reno-protective effect in cisplatin induced nephrotoxicity. *Drug Deliv*, 29(1):1848-1862. https://doi.org/10.1080/10717544.2022.2083725

Ansari MN, Rehman NU, Karim A, et al., 2021. Role of oxidative stress and inflammatory cytokines (TNF-α and IL-6) in acetic acid-induced ulcerative colitis in rats: ameliorated by *Otostegia fruticosa*. *Life (Basel)*, 11(3):195. https://doi.org/10.3390/life11030195

Attallah NGM, Al-Fakhrany OM, Elekhnawy E, et al., 2022a. Anti-biofilm and antibacterial activities of *Cycas media* R. Br secondary metabolites: in silico, in vitro, and in vivo approaches. *Antibiotics (Basel)*, 11(8):993. https://doi.org/10.3390/antibiotics11080993

Attallah NGM, El-Sherbeni SA, El-Kadem AH, et al., 2022b. Elucidation of the metabolite profile of *Yucca gigantea* and assessment of its cytotoxic, antimicrobial, and anti-inflammatory activities. *Molecules*, 27(4):1329. https://doi.org/10.3390/molecules27041329

Aziz N, Kim MY, Cho JY, 2018. Anti-inflammatory effects of luteolin: a review of in vitro, in vivo, and in silico studies. *J Ethnopharmacol*, 225:342-358. https://doi.org/10.1016/j.jep.2018.05.019

Bancroft JD, Gamble M, 2008. Theory and Practice of Histological Techniques, 6th Ed. Churchill Livingstone, Philadelphia, USA.

Ben-Horin S, Novack L, Mao R, et al., 2022. Efficacy of biologic drugs in short-duration versus long-duration inflammatory bowel disease: a systematic review and an individual-patient data meta-analysis of randomized controlled trials. *Gastroenterology*, 162(2):482-494. https://doi.org/10.1053/j.gastro.2021.10.037

Bertevello PL, Logullo ÂF, Nonogaki S, et al., 2005. Immunohistochemical assessment of mucosal cytokine profile in acetic acid experimental colitis. *Clinics (Sao Paulo)*, 60(4):277-286. https://doi.org/10.1590/s1807-59322005000400004

Blacher E, Levy M, Tatirovsky E, et al., 2017. Microbiome-modulated metabolites at the interface of host immunity. *J Immunol*, 198(2):572-580. https://doi.org/10.4049/jimmunol.1601247

Bruscoli S, Febo M, Riccardi C, et al., 2021. Glucocorticoid therapy in inflammatory bowel disease: mechanisms and clinical practice. *Front Immunol*, 12:691480. https://doi.org/10.3389/fimmu.2021.691480

Checa J, Aran JM, 2020. Reactive oxygen species: drivers of physiological and pathological processes. *J Inflamm Res*, 13:1057-1073. https://doi.org/10.2147/JIR.S275595

Dignass A, Eliakim R, Magro F, et al., 2012. Second European evidence-based consensus on the diagnosis and management of ulcerative colitis part 1: definitions and diagnosis. *J Crohns Colitis*, 6(10):965-990. https://doi.org/10.1016/j.crohns.2012.09.003

Elekhnawy E, Negm WA, 2022. The potential application of probiotics for the prevention and treatment of COVID-19. *Egypt J Med Hum Genet*, 23:36. https://doi.org/10.1186/s43042-022-00252-6

Elmongy EI, Negm WA, Elekhnawy E, et al., 2022. Antidiarrheal and antibacterial activities of Monterey cypress phytochemicals: in vivo and in vitro approach. *Molecules*, 27(2):346. https://doi.org/10.3390/molecules27020346

Fan MM, Xiang G, Chen JW, et al., 2020. Libertellenone M, a diterpene derived from an endophytic fungus *Phomopsis* sp. S12, protects against DSS-induced colitis via inhibiting both nuclear translocation of NF-κB and NLRP3 inflammasome activation. *Int Immunopharmacol*, 80:106144. https://doi.org/10.1016/j.intimp.2019.106144

Gautam MK, Goel S, Ghatule RR, et al., 2013. Curative effect of *Terminalia chebula* extract on acetic acid-induced experimental colitis: role of antioxidants, free radicals and acute inflammatory marker. *Inflammopharmacology*, 21(5):377-383. https://doi.org/10.1007/s10787-012-0147-3

Hsiao YP, Chen HL, Tsai JN, et al., 2021. Administration of *Lactobacillus reuteri* combined with *Clostridium butyricum* attenuates cisplatin-induced renal damage by gut microbiota reconstitution, increasing butyric acid production, and suppressing renal inflammation. *Nutrients*, 13(8):2792. https://doi.org/10.3390/nu13082792

Kaur L, Gordon M, Baines PA, et al., 2020. Probiotics for induction of remission in ulcerative colitis. *Cochrane Database Syst Rev*, 3(3):CD005573. https://doi.org/10.1002/14651858.CD005573.pub3

Khairy H, Saleh H, Badr AM, et al., 2018. Therapeutic efficacy of osthole against dinitrobenzene sulphonic acid induced-colitis in rats. *Biomed Pharmacother*, 100:42-51. https://doi.org/10.1016/j.biopha.2018.01.104

Khare T, Palakurthi SS, Shah BM, et al., 2020. Natural product-based nanomedicine in treatment of inflammatory bowel disease. *Int J Mol Sci*, 21(11):3956. https://doi.org/10.3390/ijms21113956

Lane DJ, 1991. 16S/23S rRNA sequencing. *In*: Stackebrandt E, Goodfellow M (Eds.), Nucleic Acid Techniques in Bacterial Systematics. John Wiley & Sons, Chichester, p.115-147.

Lavelle A, Sokol H, 2020. Gut microbiota-derived metabolites as key actors in inflammatory bowel disease. *Nat Rev Gastroenterol Hepatol*, 17(4):223-237. https://doi.org/10.1038/s41575-019-0258-z

le Loupp AG, Bach-Ngohou K, Bourreille A, et al., 2015. Activation of the prostaglandin D2 metabolic pathway in Crohn's disease: involvement of the enteric nervous system. *BMC Gastroenterol*, 15:112. https://doi.org/10.1186/s12876-015-0338-7

Li X, Liu X, Zhang YF, et al., 2020. Protective effect of *Gloeostereum incarnatum* on ulcerative colitis via modulation of Nrf2/NF-κB signaling in C57BL/6 mice. *Mol Med*

Rep, 22(4):3418-3428. https://doi.org/10.3892/mmr.2020.11420

Liu XL, Dong MS, Chen XH, et al., 2007. Antioxidant activity and phenolics of an endophytic *Xylaria* sp. from *Ginkgo biloba. Food Chem*, 105(2):548-554. https://doi.org/10.1016/j.foodchem.2007.04.008

Liu Y, Wei WH, Liang SW, et al., 2022. Esculentoside A could attenuate apoptosis and inflammation in TNBS-induced ulcerative colitis via inhibiting the nuclear translocation of NF-κB. *Ann Transl Med*, 10(14):771. https://doi.org/10.21037/atm-22-2675

Livak KJ, Schmittgen TD, 2001. Analysis of relative gene expression data using real-time quantitative PCR and the $2^{-\Delta\Delta C_T}$ method. *Methods*, 25(4):402-408. https://doi.org/10.1006/meth.2001.1262

Mi H, Liu FB, Li HW, et al., 2017. Anti-inflammatory effect of Chang-An-Shuan on TNBS-induced experimental colitis in rats. *BMC Complement Altern Med*, 17:315. https://doi.org/10.1186/s12906-017-1794-0

Peyrottes A, Coquant G, Brot L, et al., 2020. Anti-inflammatory effects of analogues of *N*-acyl homoserine lactones on eukaryotic cells. *Int J Mol Sci*, 21(24):9448. https://doi.org/10.3390/ijms21249448

Piechota-Polanczyk A, Fichna J, 2014. Review article: the role of oxidative stress in pathogenesis and treatment of inflammatory bowel diseases. *Naunyn Schmiedebergs Arch Pharmacol*, 387(7):605-620. https://doi.org/10.1007/s00210-014-0985-1

Popov J, Caputi V, Nandeesha N, et al., 2021. Microbiota-immune interactions in ulcerative colitis and colitis associated cancer and emerging microbiota-based therapies. *Int J Mol Sci*, 22(21):11365. https://doi.org/10.3390/ijms222111365

Quettier-Deleu C, Gressier B, Vasseur J, et al., 2000. Phenolic compounds and antioxidant activities of buckwheat (*Fagopyrum esculentum* Moench) hulls and flour. *J Ethnopharmacol*, 72(1-2):35-42. https://doi.org/10.1016/s0378-8741(00)00196-3

Raish M, Shahid M, Bin Jardan YA, et al., 2021. Gastroprotective effect of sinapic acid on ethanol-induced gastric ulcers in rats: involvement of Nrf2/HO-1 and NF-κB signaling and antiapoptotic role. *Front Pharmacol*, 12:622815. https://doi.org/10.3389/fphar.2021.622815

Ran ZH, Chen C, Xiao SD, 2008. Epigallocatechin-3-gallate ameliorates rats colitis induced by acetic acid. *Biomed Pharmacother*, 62(3):189-196. https://doi.org/10.1016/j.biopha.2008.02.002

Rana KL, Kour D, Kaur T, et al., 2020. Endophytic microbes: biodiversity, plant growth-promoting mechanisms and potential applications for agricultural sustainability. *Antonie van Leeuwenhoek*, 113(8):1075-1107. https://doi.org/10.1007/s10482-020-01429-y

Shahid M, Raish M, Ahmad A, et al., 2022. Sinapic acid ameliorates acetic acid-induced ulcerative colitis in rats by suppressing inflammation, oxidative stress, and apoptosis. *Molecules*, 27(13):4139. https://doi.org/10.3390/molecules27134139

Singh M, Kumar A, Singh R, et al., 2017. Endophytic bacteria: a new source of bioactive compounds. *3Biotech*, 7(5):315. https://doi.org/10.1007/s13205-017-0942-z

Strobel G, Daisy B, 2003. Bioprospecting for microbial endophytes and their natural products. *Microbiol Mol Biol Rev*, 67(4):491-502. https://doi.org/10.1128/MMBR.67.4.491-502.2003

Twaij BM, Hasan MN, 2022. Bioactive secondary metabolites from plant sources: types, synthesis, and their therapeutic uses. *Int J Plant Biol*, 13(1):4-14. https://doi.org/10.3390/ijpb13010003

Vavricka SR, Brun L, Ballabeni P, et al., 2011. Frequency and risk factors for extraintestinal manifestations in the Swiss inflammatory bowel disease cohort. *Am J Gastroenterol*, 106(1):110-119. https://doi.org/10.1038/ajg.2010.343

Wang D, DuBois RN, 2010. The role of COX-2 in intestinal inflammation and colorectal cancer. *Oncogene*, 29(6):781-788. https://doi.org/10.1038/onc.2009.421

Wang QH, Zhi TX, Han PP, et al., 2021. Potential anti-inflammatory activity of walnut protein derived peptide leucine-proline-phenylalanine in lipopolysaccharides-irritated RAW264.7 cells. *Food Agric Immunol*, 32(1):663-678. https://doi.org/10.1080/09540105.2021.1982870

Xue JC, Yuan S, Hou XT, et al., 2023. Natural products modulate NLRP3 in ulcerative colitis. *Front Pharmacol*, 14:1265825. https://doi.org/10.3389/fphar.2023.1265825

Supplementary information

Table S1; Figs. S1–S3; Materials and methods